Supporting Information

Influence of Proton Acceptors on the Proton-Coupled Electron Transfer Reaction Kinetics of a Ruthenium–Tyrosine Complex

J. Christian Lennox and Jillian L. Dempsey*

Department of Chemistry, University of North Carolina, Chapel Hill, NC 27599-3290

*Correspondence to dempseyj@email.unc.edu

Table of Contents

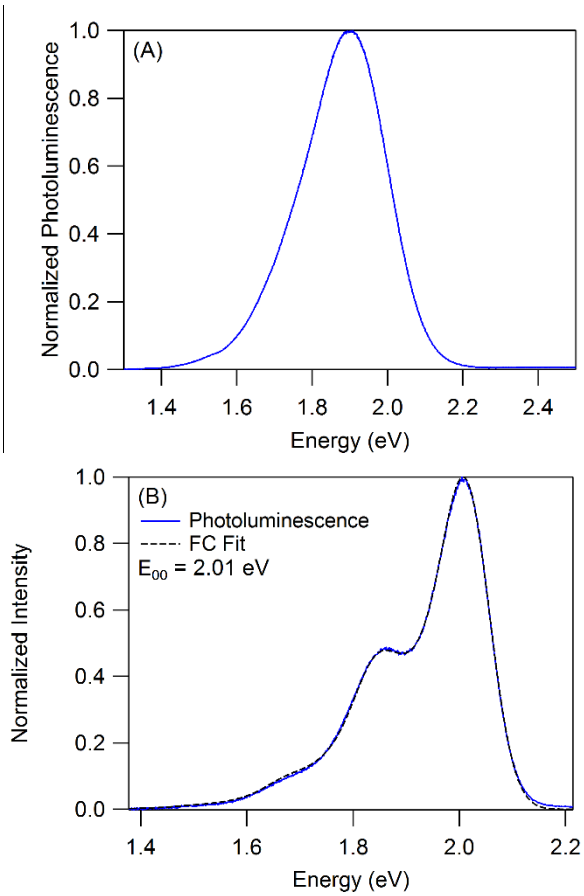

Figure S1: **(A)** Steady-state photoluminescence of $[Ru(flpy)_2(bpy\text{-}tyrOH)]^{2+}$ in acetonitrile at room temperature. λ_{ex} = 405 nm. and **(B)** Steady-state photoluminescence of [Ru(flpy)2(bpy-tyrOH)]$^{2+}$ in 2-methyltetrahydrofuran at 77 K. Franck-Condon analysis gives E_{00} of 2.01 eV. λ_{ex} = 365 nm.

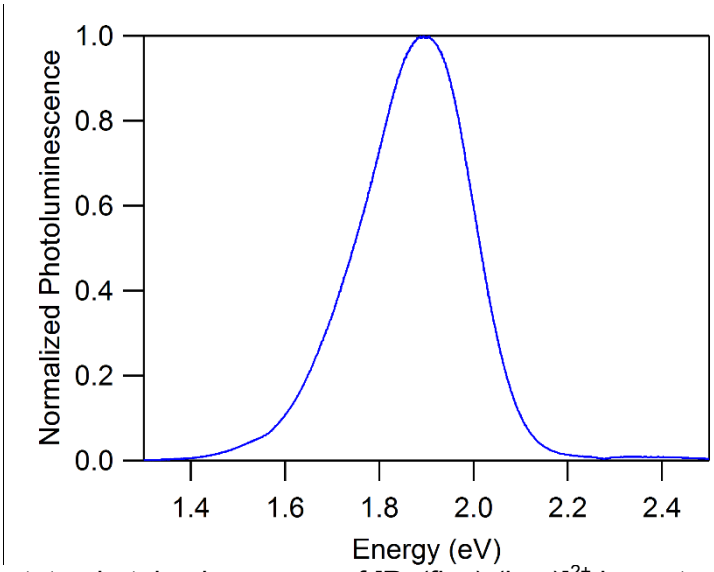

Figure S2: Steady-state photoluminescence of $[Ru(flpy)_2(bpy)]^{2+}$ in acetonitrile at room temperature. λ_{ex} = 405 nm.

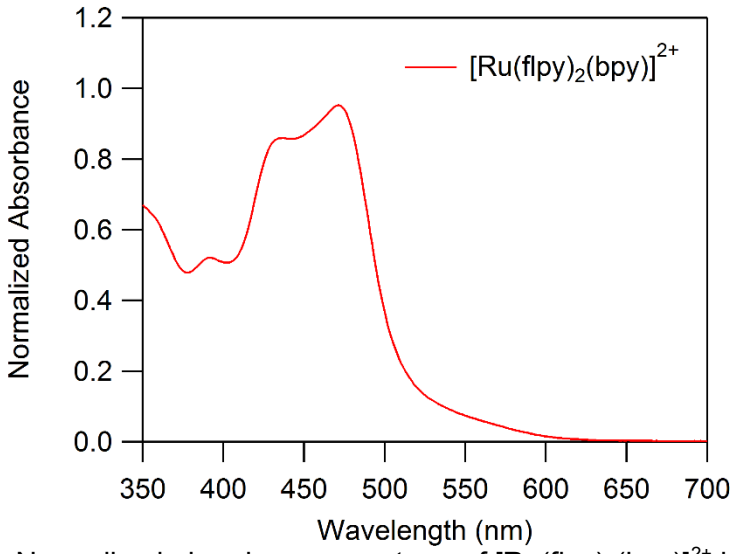

Figure S3: Normalized absorbance spectrum of $[Ru(flpy)_2(bpy)]^{2+}$ in acetonitrile.

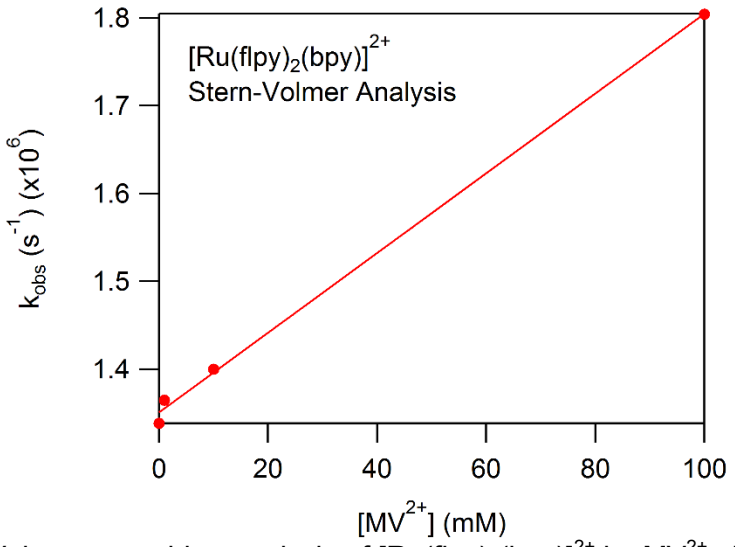

Figure S4: Stern-Volmer quenching analysis of $[Ru(flpy)_2(bpy)]^{2+}$ by MV^{2+} gives $k_q = 4.54 \times 10^6$ M^{-1} s^{-1} and $k_0 = 1.35 \times 10^6$ s^{-1}. 0.1 M $[NBu_4][PF_6]$ acetonitrile solution.

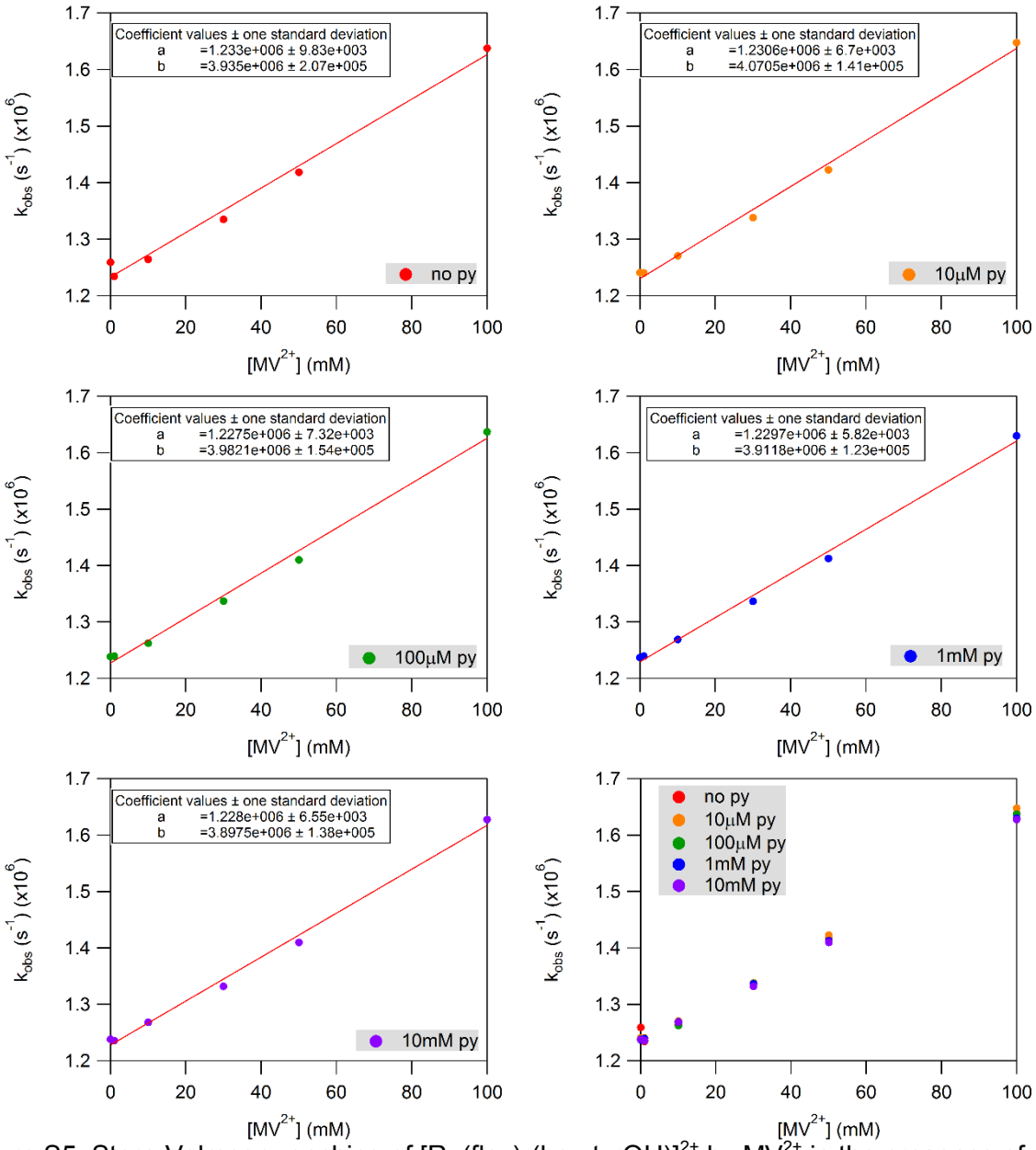

Figure S5: Stern-Volmer quenching of $[Ru(flpy)_2(bpy\text{-}tyrOH)]^{2+}$ by MV^{2+} in the presence of varying concentrations of pyridine yields an average k_q = 3.96 x 10^6 M^{-1} s^{-1} and average k_0 = 1.23 x 10^6 s^{-1}. No significant difference in the quenching rate constant k_q is observed when pyridine is present.

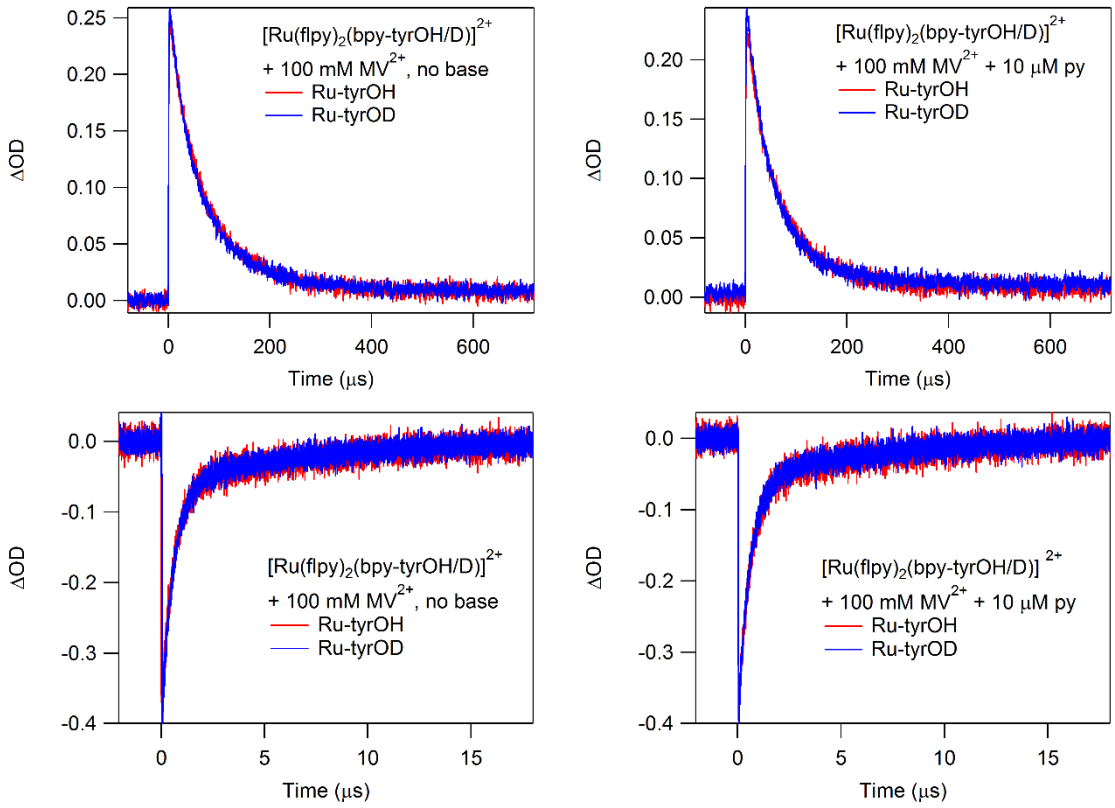

Figure S6: Kinetics traces for $[Ru(flpy)_2(bpy\text{-}tyrOH)]^{2+}$ (red) and $[Ru(flpy)_2(bpy\text{-}tyrOD)]^{2+}$ (blue) with 100 mM MV^{2+} show no change between the proteo- and deutero- species in samples without base or with 10 μM pyridine. λ_{ex} = 475 nm, λ_{obs} = 397 nm (top traces), λ_{obs} = 440 nm (bottom traces), 0.1 M $[NBu_4][PF_6]$ acetonitrile solution.

$[Ru(flpy)_2(bpy\text{-}tyrOD)]^{2+}$ was prepared by stirring in methanol-d_4 for 2 days in a nitrogen glovebox. After drying under vacuum, it was used to prepare TA samples in rigorously dried acetonitrile. No discernable differences in reaction kinetics were observed.

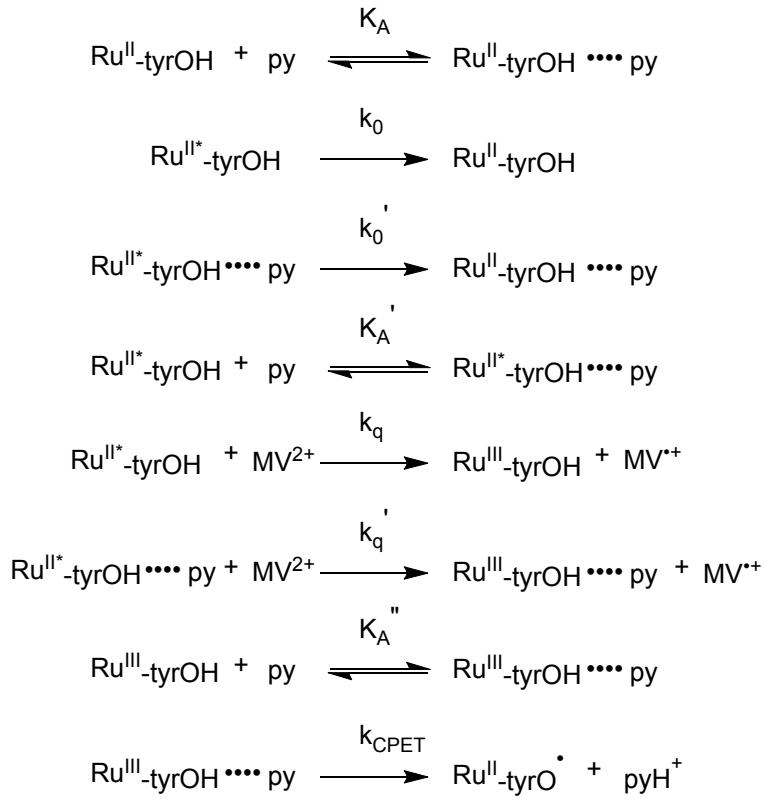

Scheme S1: CPET kinetics model for tyrosine oxidation. Note that this model was only used to investigate 440 nm kinetics and was not extended to incorporate methyl viologen back electron transfer pathways monitored at 397 nm.

As there are no significant changes in k_0 or k_q for $[Ru(flpy)_2(bpy\text{-}tyrOH)]^{2+}$ in the presence of pyridine (Figure S5), it is assumed that $k_0 = k_0'$ and $k_q = k_q'$. Furthermore, as is commonly assumed, $K_A = K_A' = K_A''$,[1,2] although recently other treatments have also been applied.[3]

$$\frac{d[Ru^{II*}\text{-}tyrOH]}{dt} = -k_0[Ru^{II*}\text{-}tyrOH] - k_q[Ru^{II*}\text{-}tyrOH][MV^{2+}] - k_A'[Ru^{II*}\text{-}tyrOH][py] + k_A'^{-1}[Ru^{II*}\text{-}tyrOH \cdots py]$$

$$\frac{d[Ru^{II*}\text{-}tyrOH \cdots py]}{dt} = -k_0[Ru^{II*}\text{-}tyrOH \cdots py] - k_q[Ru^{II*}\text{-}tyrOH \cdots py][MV^{2+}] + k_A'[Ru^{II*}\text{-}tyrOH][py] - k_A'^{-1}[Ru^{II*}\text{-}tyrOH \cdots py]$$

$$\frac{d[Ru^{III}\text{-}tyrOH]}{dt} = +k_q[Ru^{II*}\text{-}tyrOH][MV^{2+}] - k_A''[Ru^{III}\text{-}tyrOH][py] + k_A''^{-1}[Ru^{III}\text{-}tyrOH \cdots py]$$

$$\frac{d[Ru^{III}\text{-}tyrOH \cdots py]}{dt} = +k_q[Ru^{II*}\text{-}tyrOH \cdots py][MV^{2+}] + k_A''[Ru^{III}\text{-}tyrOH][py]$$

$$-k_A{}''^{-1}[Ru^{III}\text{-}tyrOH \cdots py] - k_{CPET}[Ru^{III}\text{-}tyrOH \cdots py]$$

$$\frac{d[Ru^{II}\text{-}tyrO^{\bullet}]}{dt} = +k_{CPET}[Ru^{III}\text{-}tyrOH \cdots py]$$

Scheme S2: Differential equations used in CPET kinetics model.

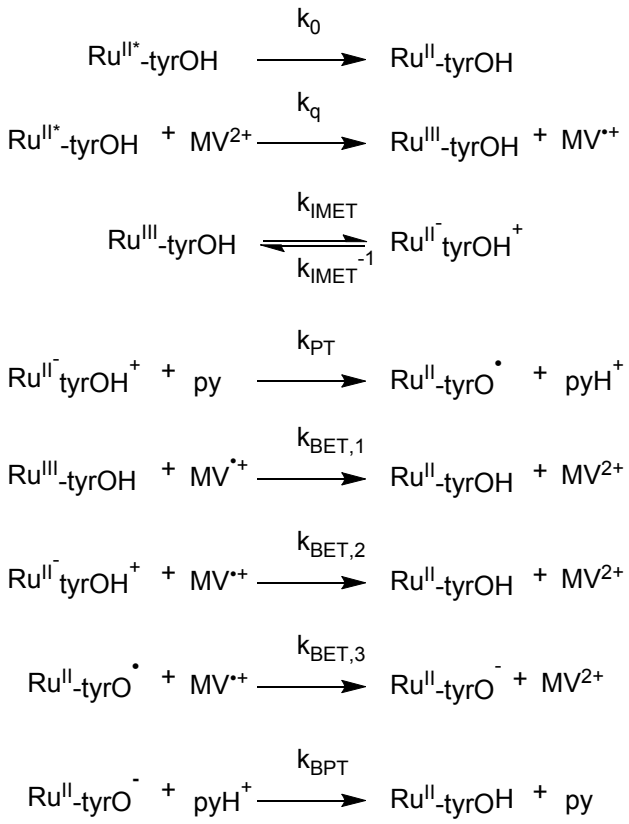

Scheme S3: Equilibrium ET-PT kinetics model for tyrosine oxidation used in scheme 6.

$$\frac{d[Ru^{II}\text{-}tyrOH]}{dt} = +k_0[Ru^{II*}\text{-}tyrOH] + k_{BET,1}[Ru^{III}\text{-}tyrOH][MV^{\bullet+}] + k_{BET,2}[Ru^{II}\text{-}tyrOH^+][MV^{\bullet+}] + k_{BPT}[Ru^{II}\text{-}tyrO^-][pyH^+]$$

$$\frac{d[Ru^{II*}\text{-}tyrOH]}{dt} = -k_0[Ru^{II*}\text{-}tyrOH] - k_q[Ru^{II*}\text{-}tyrOH][MV^{2+}]$$

$$\frac{d[Ru^{III}\text{-}tyrOH]}{dt} = +k_q[Ru^{II*}\text{-}tyrOH][MV^{2+}] - k_{BET,1}[Ru^{III}\text{-}tyrOH][MV^{\bullet+}] - k_{IMET}[Ru^{III}\text{-}tyrOH] + k_{IMET}^{-1}[Ru^{II}\text{-}tyrOH^+]$$

$$\frac{d[Ru^{II}\text{-}tyrOH^+]}{dt} = +k_{IMET}[Ru^{III}\text{-}tyrOH] - k_{IMET}^{-1}[Ru^{II}\text{-}tyrOH^+] - k_{BET,2}[Ru^{II}\text{-}tyrOH^+][MV^{\bullet+}] - k_{PT}[Ru^{II}\text{-}tyrOH^+][py]$$

$$\frac{d[Ru^{II}\text{-}tyrOH^{\bullet}]}{dt} = +k_{PT}[Ru^{II}\text{-}tyrOH^+][py] - k_{BET,3}[Ru^{II}\text{-}tyrOH^{\bullet}][MV^{\bullet+}]$$

$$\frac{d[MV^{2+}]}{dt} = -k_q[Ru^{II*}\text{-}tyrOH][MV^{2+}] + k_{BET,1}[Ru^{III}\text{-}tyrOH][MV^{\bullet+}] + k_{BET,2}[Ru^{II}\text{-}tyrOH^+][MV^{\bullet+}] + k_{BET,3}[Ru^{II}\text{-}tyrOH^{\bullet}][MV^{\bullet+}]$$

$$\frac{d[MV^{\bullet+}]}{dt} = +k_q[Ru^{II*}\text{-}tyrOH][MV^{2+}] - k_{BET,1}[Ru^{III}\text{-}tyrOH][MV^{\bullet+}] - k_{BET,2}[Ru^{II}\text{-}tyrOH^+][MV^{\bullet+}] - k_{BET,3}[Ru^{II}\text{-}tyrOH^{\bullet}][MV^{\bullet+}]$$

$$\frac{d[py]}{dt} = -k_{PT}[Ru^{II}\text{-}tyrOH^+][py] + k_{BPT}[Ru^{II}\text{-}tyrO^-][pyH^+]$$

$$\frac{d[pyH^+]}{dt} = +k_{PT}[Ru^{II}\text{-}tyrOH^+][py] - k_{BPT}[Ru^{II}\text{-}tyrO^-][pyH^+]$$

$$\frac{d[Ru^{II}\text{-}tyrO^-]}{dt} = +k_{BET,3}[Ru^{II}\text{-}tyrOH^{\bullet}][MV^{\bullet+}] - k_{BPT}[Ru^{II}\text{-}tyrO^-][pyH^+]$$

Scheme S4: Differential equations used in equilibrium ET-PT kinetics model

Table S1: Extinction Coefficients used in Kinetics Models

Species	ε at 397 nm (M^{-1} cm^{-1})	ε at 440 nm (M^{-1} cm^{-1})
MV^{2+}	0	0
$MV^{\bullet+}$	41800	0
Ru^{2+}	0	14180
Ru^{2+*}	0*	3760
Ru^{3+}	0†	2000
tyrOH	0	0
$tyrOH^{\bullet+}$	0‡	0
$tyrO^{\bullet}$	0‡	0
py	0	0
pyH^{+}	0	0

*As the Ru^{2+}/Ru^{2+*} isosbestic point for most excited $[Ru(bpy)_3]^{2+}$ complexes falls near 397 nm, and TA only measures differences in absorbance, these values are approximated to be 0.
†The change in extinction coefficient from Ru^{2+}/Ru^{2+*} to Ru^{3+} at 397 nm (ca. 400 M^{-1} cm^{-1}) is insignificant relative to the large extinction coefficient of $MV^{\bullet+}$ and was approximated as 0.[4]
‡Phenol radicals typically exhibit extinction coefficients of ca. 3200 M^{-1} cm^{-1} at peaks ranging from 385-405 nm, which are also insignificant relative to the extinction coefficient of $MV^{\bullet+}$ and was not considered in these kinetics simulations.[5]

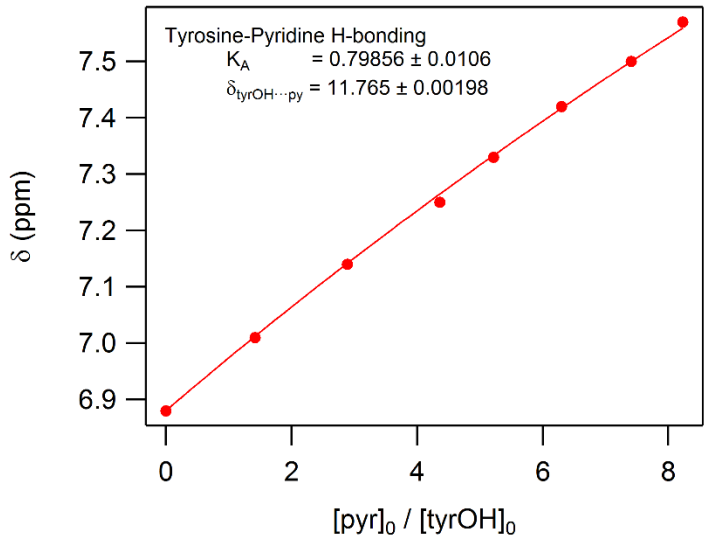

Figure S7: Tyrosine-pyridine hydrogen bonding in acetonitrile as quantified from ^{1}H NMR shift of the phenolic proton (δ) upon addition of pyridine. Tyrosine concentration was held constant at 25mM.

The association constant was found via a two-parameter fit for K_A and $\delta_{tyrOH\cdots py}$, the chemical shift of the hydrogen bound tyrosine-pyridine complex at infinite pyridine concentration, per the procedure described in reference 2.[2]

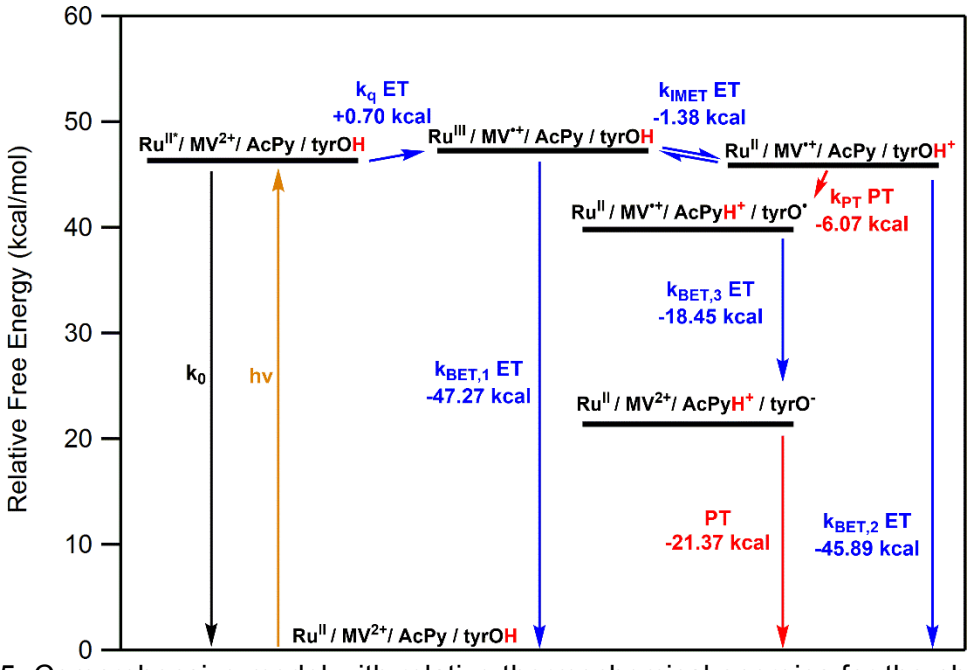

Scheme S5: Comprehensive model with relative thermochemical energies for the photoinduced reactivity of $[Ru(flpy)_2(bpy\text{-}tyrOH)]^{2+}$ with MV^{2+} and 3-acetylpyridine. pK_a of 3-acetylpyridinium = 10.75 in acetonitrile.

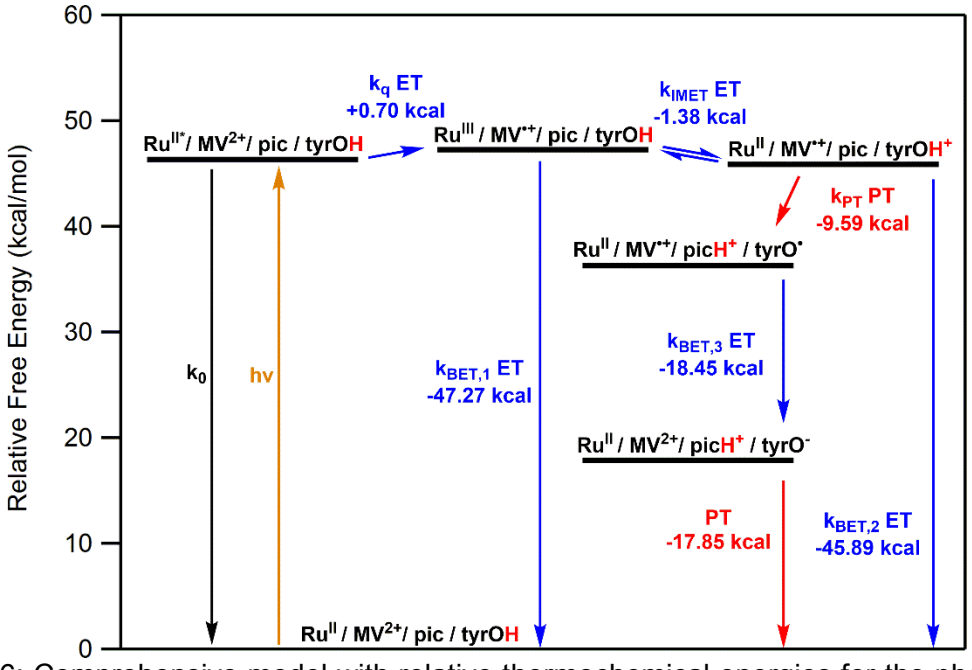

Scheme S6: Comprehensive model with relative thermochemical energies for the photoinduced reactivity of $[Ru(flpy)_2(bpy\text{-}tyrOH)]^{2+}$ with MV^{2+} and 2-picoline. pK_a of 2-picolinium = 13.32 in acetonitrile.

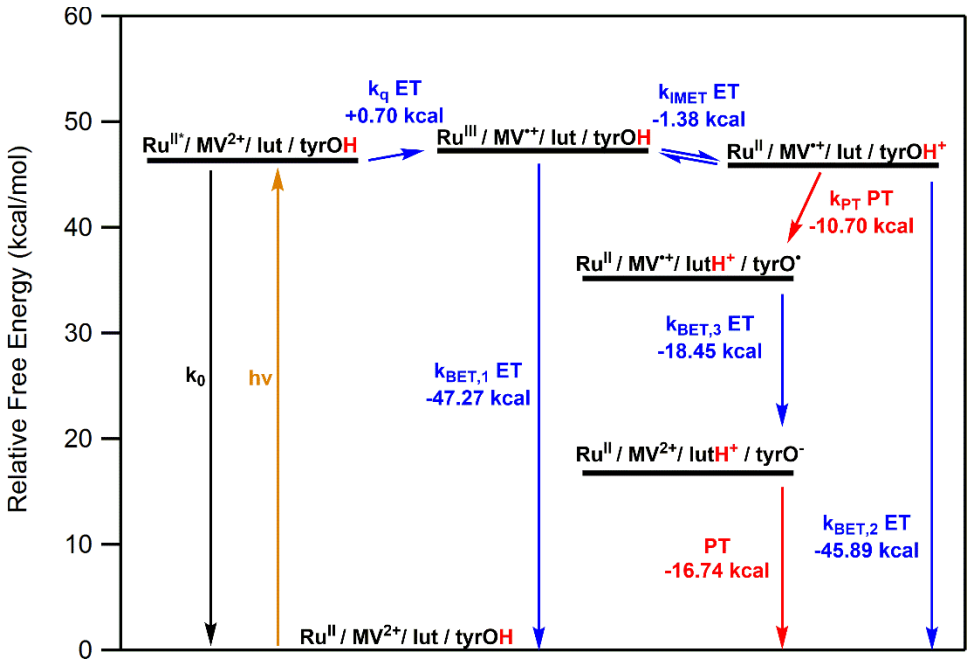

Scheme S7: Comprehensive model with relative thermochemical energies for the photoinduced reactivity of $[Ru(flpy)_2(bpy\text{-}tyrOH)]^{2+}$ with MV^{2+} and 2,6-lutidine. pK_a of 2,6-lutidinium = 14.13 in acetonitrile.

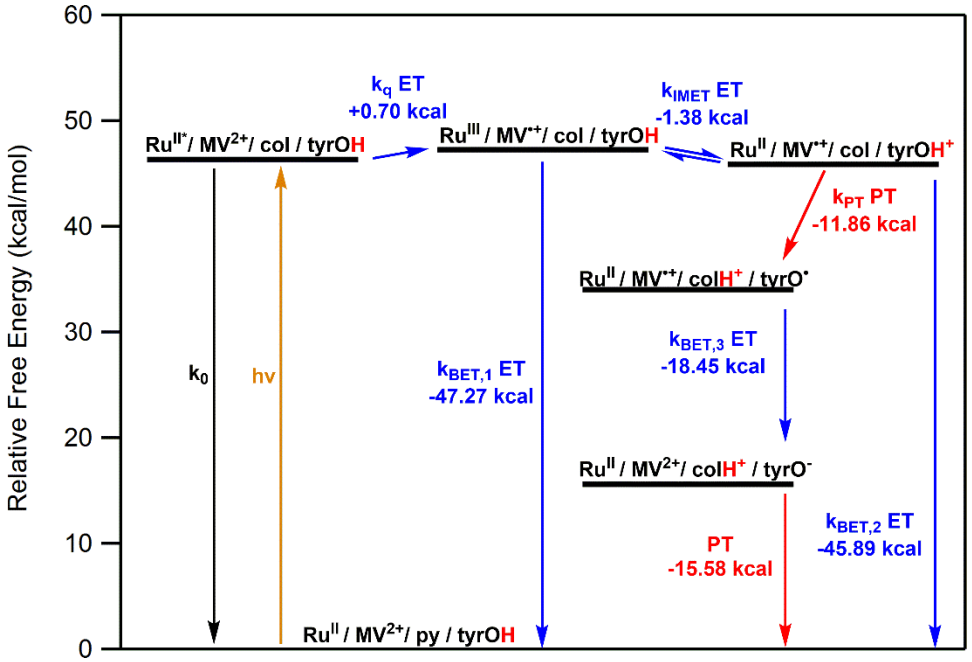

Scheme S8: Comprehensive model with relative thermochemical energies for the photoinduced reactivity of $[Ru(flpy)_2(bpy\text{-}tyrOH)]^{2+}$ with MV^{2+} and 2,4,6-collidine. pK_a of 2,4,6-collidinium = 14.98 in acetonitrile.

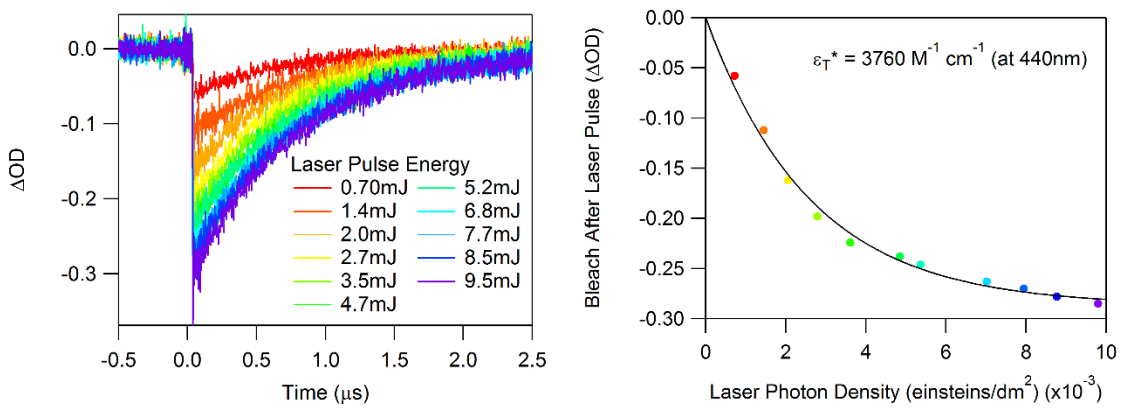

Figure S8: Ruthenium bleach intensity at 440 nm of 16 μM $[Ru(flpy)_2(bpy\text{-}tyrOH)]^{2+}$ as a function of laser pulse energy yields the triplet excited-state extinction coefficient of $[Ru(flpy)_2(bpy\text{-}tyrOH)]^{2+*}$. λ_{ex} = 475 nm, λ_{obs} = 440 nm, 0.1 M $[NBu_4][PF_6]$.

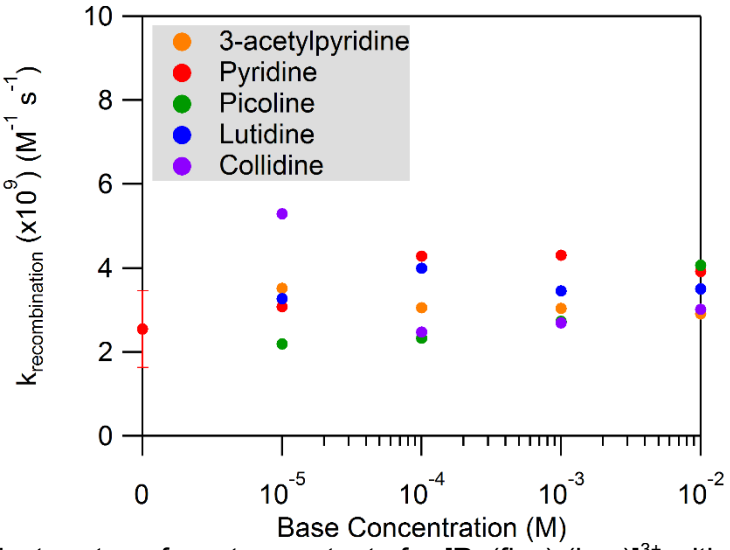

Figure S9: Back electron transfer rate constants for $[Ru(flpy)_2(bpy)]^{3+}$ with $MV^{\bullet+}$ in the presence of various concentrations of substituted pyridines. Samples containing ca. 40 μM $[Ru(flpy)_2(bpy)]^{2+}$, 100 mM MV^{2+}, and varying concentrations of pyridines were excited, yielding $[Ru(flpy)_2(bpy)]^{3+}$ and $MV^{\bullet+}$. The subsequent recombination was tracked via TA at 397 nm. From second-order equal concentration kinetics, $1/[MV^{\bullet+}] = k_{BET} \cdot t + C$. By converting the traces to 1/ΔOD, fitting to a straight line, and multiplying the slope by the change in extinction coefficient ($\Delta\varepsilon_{397}$ for $MV^{\bullet+}/MV^{2+}$ = 41800 M^{-1} cm^{-1}), we obtain the rate of back electron transfer, k_{BET}. λ_{ex} = 475 nm, λ_{obs} = 397 nm, 0.1 M $[NBu_4][PF_6]$.

These data illustrate that the recombination kinetics are not significantly influenced by the presence of pyridine bases at the concentrations used in this study The average rate constant in the absence of pyridine is 2.5 ± 0.9 x 10^9 M^{-1} s^{-1}. For comparison, the average value for all data (across all substituted pyridines and concentrations evaluated) is 3.57 x 10^9 M^{-1} s^{-1}. The pyridine-free data was used as $k_{BET,1}$ in the kinetics modeling of $[Ru(flpy)_2(bpy\text{-}tyrOH)]^{2+}$.

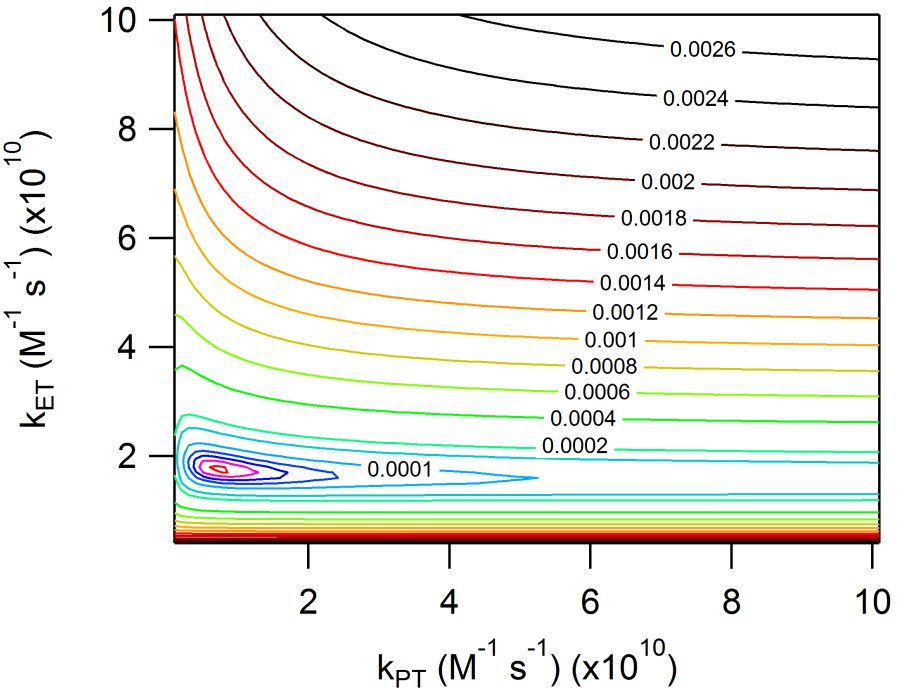

Figure S10: Example dataset of raw residual values from 2-parameter fitting of $k_{BET,3}$ (k_{ET} on the y-axis above) and k_{PT} (x-axis) as described in the main text. Each rate constant was varied systematically across 100 values between 10^9 and 10^{11}, producing 10,000 different combinations. Using the kinetics model, a simulation transient absorption trace was produced using each of these 10,000 combinations at four different base concentrations, and this simulated data compared to an experimental dataset containing traces at each of those base concentrations. The residuals resulting from differences between the simulated and experimental data were then plotted to find the minimum. In this example dataset, [pyridine] = 10 μM, 100 μM, 1 mM, 10 mM, and the lowest residual values result from k_{PT} = 5.5 x 10^9 M^{-1} s^{-1} and k_{ET} = 1.9 x 10^{10} M^{-1} s^{-1}.

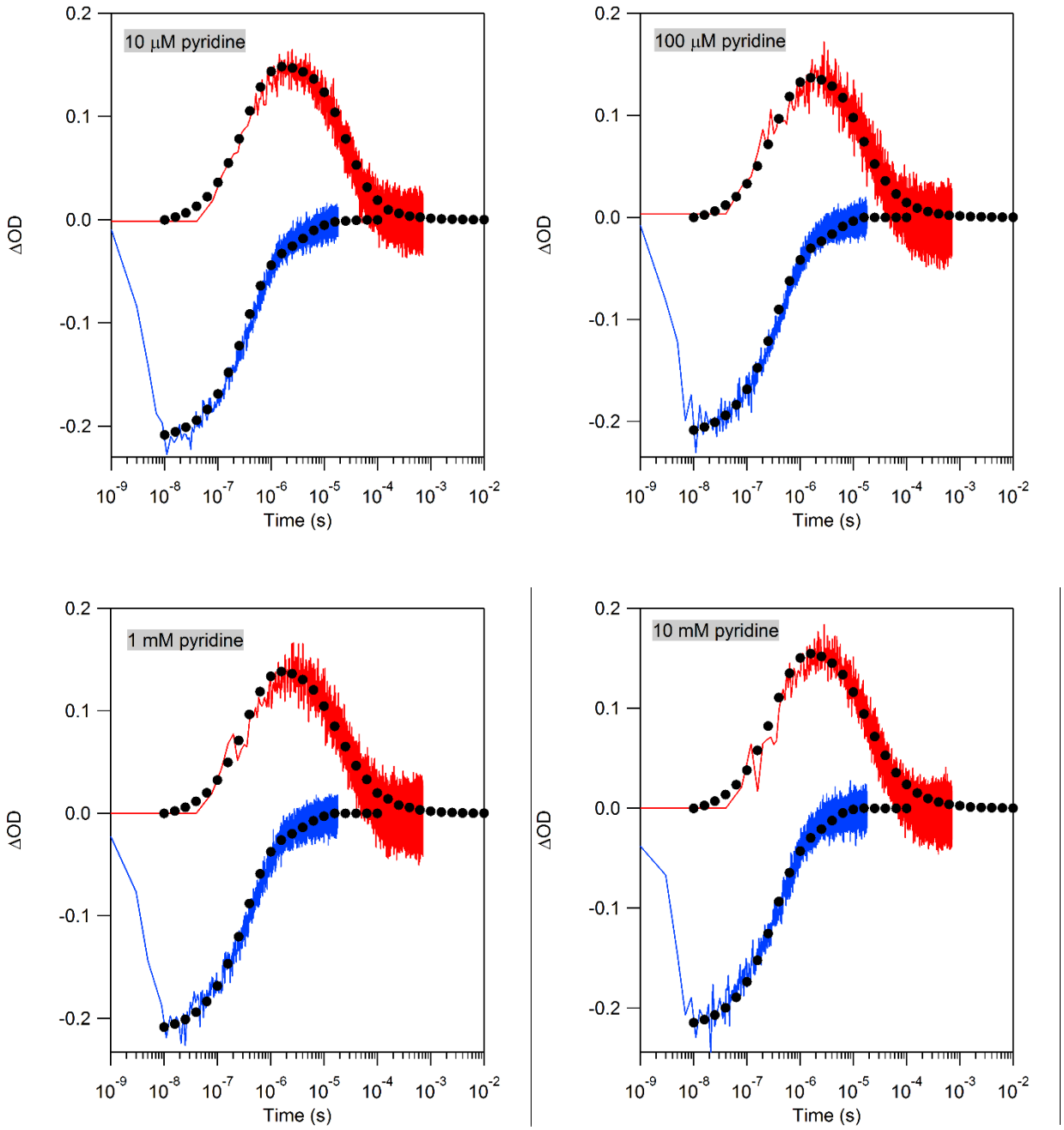

Figure S11: Example transient absorption traces of $[Ru(flpy)_2(bpy\text{-}tyrOH)]^{2+}$ with 100 mM MV^{2+} with various concentrations of pyridine base at λ_{obs} = 440 nm (blue trace) and λ_{obs} = 397 nm (red trace) and corresponding kinetics models (markers). λ_{ex} = 475 nm.

Table S2: Comparison of ET driving force for an ET-PT mechanism and operative PCET mechanism for selected oxidative PCET systems in organic solvents and water-organic solvent mixtures as reported in the literature.

Ref.	Assigned Mechanism	ΔG_{ET} for ET-PT mechanism (kcal/mol)	Oxidant	Base	Substrate
6	CPET	+8.8	$[Fe(MeObpy)_3]^{3+}$	pyridine	$W(Cp)(CO)_3H$
	CPET	+5.3	$[Fe(dmbpy)_3]^{3+}$		
	CPET	+1.8	$[Fe(bpy)_3]^{3+}$		
	ET-PT	+0.23	$[Ru(dmbpy)_3]^{3+}$		
7	CPET	+16.8	$[Re(CO)_3(bpz)(py)]^{+}$	bpz	4-cyanophenol
	CPET	+8.8	$[Re(CO)_3(bpy)(pz)]^{+}$	pz	
8	CPET	0	$[Ru(bpy)_2(bpy\text{-}xy_1\text{-}^{dtb}PhOH)]^{3+}$	imidazole	$^{dtb}PhOH$ [c]
	CPET	0	$[Ru(bpy)_2(bpy\text{-}xy_2\text{-}^{dtb}PhOH)]^{3+}$		
9	CPET	+11.5	$[Ru(bpy)_2(bpy\text{-}xy_1\text{-}^{dtb}PhOH)]^{2+*}$	pyrrolidine	$^{dtb}PhOH$ [c]
	CPET	+11.5	$[Ru(bpy)_2(bpy\text{-}xy_2\text{-}^{dtb}PhOH)]^{2+*}$		
	CPET	+11.5	$[Ru(bpy)_2(bpy\text{-}xy_3\text{-}^{dtb}PhOH)]^{2+*}$		
10	ET-PT	+3.0	$[Ru(bpz)_3]^{2+*}$	bpz	4-methoxyphenol
	CPET	+7.1			4-bromophenol
	CPET	+7.6			4-chlorophenol
	CPET	+7.6			phenol
	CPET	+11.1			4-cyanophenol
11	ET-PT	+0.69	$[Ru(bpz)_3]^{2+*}$	bpz	$2,4,6\text{-}Me_3PhSH$
	CPET or PT-ET	+18.4			$2,4,6\text{-}Cl_3PhSH$
	PT-ET	>25			F_5PhSH
2	CPET	+3.5	$[Ru(flpy)_3]^{2+*}$	pyridine	4-methoxyphenol
	CPET	+6.0			4-methylphenol
	CPET	+7.6			4-bromophenol
	CPET	+8.1			4-chlorophenol
	CPET	+8.1			phenol
	CPET	+11.5			4-cyanophenol
3[a]	ET-PT	+3.4	$[Re(CO)_3(bpy)(4,4'\text{-}bpy)]^{+*}$	4,4'-bpy	4-methoxyphenol
	ET-PT	+6.4			4-bromophenol
	CPET	+9.4			4-chlorophenol
	CPET	+9.8			phenol
	CPET	+11.9			4-cyanophenol
12[b]	ET-PT	~+5.8	$[Ru(bpz)_2(bpz\text{-}xy\text{-}PhOH)]^{2+*}$	water	phenol [c]
	CPET	~+9.2	$[Ru(bpz)_2(bpz\text{-}xy\text{-}^{CN}PhOH)]^{2+*}$		4-cyanophenol [c]

13[b]	ET-PT	~-4.6	$[Re(phen)(CO)_3(py\text{-}xy_1\text{-}^{dtb}PhOH)]^{+*}$	water	$^{dtb}PhOH$ [c]
14	CPET	~+7.9	$[Ru(bpy)_2(bpy\text{-}tyrOH\text{-}base)]^{2+}$	benzimidazole	tyrOH···base [c]
				pyridine	

bpy = 2,2'-bipyridine, MeObpy = 4,4'-dimethoxy-2,2'-bipyridine, dmbpy = 4,4'-dimethyl-2,2'bipyridine, bpz = 2,2'-bipyrazine, py = pyridine, pz = pyrazine, flpy = 4,4'-bis(trifluoromethyl)-2,2'-bipyridine, Cp = cyclopentadiene. phen = 1,10-phenanthroline, $^{dtb}PhOH$ = 2,6-di-*tert*-butylphenol, [a] conducted in 3:1 acetonitrile:water [b] conducted in 1:1 acetonitrile:water [c] covalently bonded to the oxidant.

References

(1) Ward, W. M.; Farnum, B. H.; Siegler, M.; Meyer, G. J. Chloride Ion-Pairing with Ru(II) Polypyridyl Compounds in Dichloromethane. *J. Phys. Chem. A* **2013**, *117*, 8883–8894.

(2) Nomrowski, J.; Wenger, O. S. Photoinduced PCET in Ruthenium–Phenol Systems: Thermodynamic Equivalence of Uni- and Bidirectional Reactions. *Inorg. Chem.* **2015**, *54*, 3680–3687.

(3) Dongare, P.; Bonn, A. G.; Maji, S.; Hammarström, L. Analysis of Hydrogen-Bonding Effects on Excited-State Proton-Coupled Electron Transfer from a Series of Phenols to a Re(I) Polypyridyl Complex. *J. Phys. Chem. C* **2017**, *121*, 12569–12576.

(4) Callahan, J. H.; Hool, K.; Reynolds, J. D.; Cook, K. D. Glycerol-Induced Reduction in Electrohydrodynamic Mass Spectrometry. *Anal. Chem.* **1988**, *60*, 714–719.

(5) Das, T. N. Oxidation of Phenol in Aqueous Acid: Characterization and Reactions of Radical Cations Vis-a-Vis the Phenoxyl Radical. *J. Phys. Chem. A* **2005**, *109*, 3344–3351.

(6) Bourrez, M.; Steinmetz, R.; Ott, S.; Gloaguen, F.; Hammarström, L. Concerted Proton-Coupled Electron Transfer from a Metal-Hydride Complex. *Nat. Chem.* **2015**, *7*, 140–145.

(7) Bronner, C.; Wenger, O. S. Proton-Coupled Electron Transfer between 4-Cyanophenol and Photoexcited Rhenium(I) Complexes with Different Protonatable Sites. *Inorg. Chem.* **2012**, *51*, 8275–8283.

(8) Chen, J.; Kuss-Petermann, M.; Wenger, O. S. Dependence of Reaction Rates for Bidirectional PCET on the Electron Donor–Electron Acceptor Distance in Phenol–Ru(2,2′-Bipyridine)$_3^{2+}$ Dyads. *J. Phys. Chem. B* **2015**, *119*, 2263–2273.

(9) Chen, J.; Kuss-Petermann, M.; Wenger, O. S. Distance Dependence of Bidirectional Concerted Proton-Electron Transfer in Phenol-Ru(2,2′-Bipyridine)$_3^{2+}$ Dyads. *Chem. - A Eur. J.* **2014**, *20*, 4098–4104.

(10) Bronner, C.; Wenger, O. S. Kinetic Isotope Effects in Reductive Excited-State Quenching of Ru(2,2′-bipyrazine)$_3^{2+}$ by Phenols. *J. Phys. Chem. Lett.* **2012**, *3*, 70–74.

(11) Kuss-Petermann, M.; Wenger, O. S. Mechanistic Diversity in Proton-Coupled Electron Transfer between Thiophenols and Photoexcited [Ru(2,2′-Bipyrazine)$_3$]$^{2+}$. *J. Phys. Chem. Lett.* **2013**, *4*, 2535–2539.

(12) Bronner, C.; Wenger, O. S. Long-Range Proton-Coupled Electron Transfer in phenol–Ru(2,2'-bipyrazine)$_3^{2+}$ Dyads. *Phys. Chem. Chem. Phys.* **2014**, *16*, 3617–3622.

(13) Kuss-Petermann, M.; Wolf, H.; Stalke, D.; Wenger, O. S. Influence of Donor–Acceptor Distance Variation on Photoinduced Electron and Proton Transfer in Rhenium(I)–Phenol Dyads. *J. Am. Chem. Soc.* **2012**, *134*, 12844–12854.

(14) Zhang, M. T.; Irebo, T.; Johansson, O.; Hammarström, L. Proton-Coupled Electron Transfer from Tyrosine: A Strong Rate Dependence on Intramolecular Proton Transfer Distance. *J. Am. Chem. Soc.* **2011**, *133*, 13224–13227.